Characterizing specimen induced aberrations for high NA adaptive optical microscopy

M. Schwertner, M.J. Booth and T. Wilson

Department of Engineering Science, University of Oxford, Parks Road, Oxford OX1 3PJ, UK, Fax: +44 1865 273905

Tony.Wilson@eng.ox.ac.uk

Abstract: Aberrations are known to severely compromise image quality in optical microscopy, especially when high numerical aperture (NA) lenses are used in confocal fluorescence microscopy (CFM) and two-photon microscopy (TPM). The method of adaptive optics may correct aberrations and restore diffraction limited operation. So far the problem of aberrations that occur in the imaging of biological specimens has not been quantified. However, this information is essential for the design of adaptive optics systems. We have therefore built an interferometer incorporating high NA objective lenses to measure the aberrations introduced by biological specimens. The measured wavefronts were decomposed into their Zernike mode content in order both to classify and quantify the aberrations. We calculated the potential benefit of correcting different numbers of Zernike modes using different NAs in an adaptive CFM by comparing the signal levels before and after correction. The results indicate that adaptive correction of low order Zernike modes can provide significant benefit for many specimens. The results also show that quantitative fluorescence microscopy may be strongly affected by specimen induced aberrations in non-adaptive systems.

OCIS codes: (180.5810) Scanning microscopy; (180.1790) Confocal microscopy; (010.1080) Adaptive optics

References and links

1. F. P. Bolin, L. E. Preuss, R. C. Taylor and R. J. Ference "Refractive index of some mammalian tissues using a fiber optic cladding method." Appl. Opt. **28,** 2279–2303 (1989).
2. G. J. Tearney, M. E. Brezinski, J. F. Southern, B. E. Bouma, M. R. Hee and J. G. Fujimoto "Determination of the refractive index of highly scattering human tissue by optical coherence tomography" Opt. Lett. **20,** 2258–2260 (1995).
3. A. Dunn. "Light scattering properties of cells". Dissertation, University of Texas, Austin, http://www.nmr.mgh.harvard.edu/∼adunn/papers/dissertation/node7.html, 1998.
4. S. Hell, G. Reiner, C. Cremer, and E.H.K. Stelzer. "Aberrations in confocal fluorescence microscopy induced by mismatches" in refractive index. J. Microscopy **169,** 391–405 (1993).
5. T. Wilson and A.R. Carlini. "The effects of aberrations on the axial response of confocal imaging" systems. J. Microscopy **154,** 243–256 (1989).
6. M.J. Booth, M.A.A. Neil, and T. Wilson. "Aberration correction for confocal imaging in refractive-index-mismatched media." J. Microscopy **192,** 90–98 (1998).
7. M.J. Booth and T. Wilson. "Strategies for the compensation of specimen induced aberration in confocal microscopy of skin." J. Microscopy **200,** 68–74 (2000).

#5762 - $15.00 US Received 17 November 2004; revised 13 December 2004; accepted 14 December 2004

8. P. Török, P. Varga, and G. Németh. "Analytic solution of the diffraction integrals and interpretation of wave-front distortion when light is focussed through a planar interface between materials of mismatched refractive indices." J. Opt. Soc. Am. A **12,** 2660–2671 (1995).
9. P. Török, P. Varga, Z. Laczik, and G. R. Booker. "Electromagnetic diffraction of light focused through a planar interface between materials of mismatched refractive indices: an integral representation." J. Opt. Soc. Am. A **12,** 325 (1995).
10. J.B. Pawley. "Handbook of Biological Confocal Microscopy". Plenum, New York, 1995.
11. T. Wilson and C.J.R. Sheppard. "Theory and practice of Scanning Optical Microscopy". Academic Press, London, 1984.
12. W. J. Denk, J. P. Strickler, and W. W. Webb. "Two-photon laser scanning fluorescence microscopy." Science **248,** 73–76 (1990).
13. J. W. Hardy. "Adaptive Optics for Astronomical Telescopes". Oxford University Press, 1998.
14. B.C. Platt and R. Shack. "History and priciples of Shack-Hartmann wavefront sensing." J. Refractive Surgery **17,** 573–577 (2001).
15. M. A. A. Neil, M. J. Booth, and T. Wilson. "New modal wavefront sensor: a theoretical analysis." J. Opt. Soc. Am. **17,** 1098–1107 (2000).
16. L. Zhu, P. Sun, D.U. Bartsch, W.R. Freeman, and Y. Fainman. "Adaptive control of a micromachined continuous-membrane deformable mirror for aberration compensation." Appl. Opt. **38,** 168–170 (1999).
17. G. Vdovin, P.M. Sarro, and S. Middelhoek. "Technology and applications of micromachined adaptive mirrors." J. Micromech. and Microeng. **9,** R8 (1999).
18. N. Doble, G. Yoon, L. Chen, P. Bierden, B. Singer, S. Olivier, D. R. Williams. "Use of a microelectromechanical mirror for adaptive optics in the human eye." Opt. Lett. **27,** 1537-1539 (2002).
19. "A. Roorda, F. Romero-Borja, W.J. Donnelly III, H. Queener, Thomas J. Hebert and M.C.W. Campbell. Adaptive optics scanning laser ophthalmoscopy." Opt. Express **10,** 405–411 (2002).
20. M. A. A. Neil, R. Juškaitis, M. J. Booth, T. Wilson, T. Tanaka, and S. Kawata. "Adaptive aberration correction in a two-photon microscope." J. Microscopy **200,** 105–108 (2000).
21. L. Sherman, J. Y. Ye, O. Albert, and T. B. Norris. "Adaptive correction of depth-induced aberrations in multiphoton scanning microscopy using a deformable mirror." J. Microscopy **206,** 65–71 (2002).
22. P. N. Marsh, D. Burns, and J. M. Girkin. "Practical implementation of adaptive optics in multiphoton microscopy." Opt. Express **11,** 1123–1130 (2003).
23. M.J. Booth, M. A. A. Neil, R. Juškaitis, and T. Wilson. "Adaptive aberration correction in a confocal microscope." Proceedings of the National Academy of Science 99, 5788–5792 (2002).
24. J.H. Bruning and D.R Heriott and J.E. Gallhager and D.P. Rosenfeld and A.D. White and D.J Brangaccio. "Digital Wavefront Measuring Interferometer for Testing Optical Surfaces and Lenses." Appl. Opt. **13,** 2693–2703 (1974).
25. J. E. Greivenkamp and J. H. Bruning. "Phase shifting interferometry." Optical shop testing, ed. by D. Malacara, Wiley New York, 1992.
26. M. Schwertner, M. J. Booth, M.A.A. Neil, and T. Wilson. "Measurement of specimen-induced aberrations of biological samples using phase stepping interferometry." J. Microscopy **213,** 11–19 (2004).
27. M. Schwertner, M.J. Booth, and T. Wilson. "Simulation of specimen induced aberrations for objects with spherical and cylindrical symmetry." J. Microscopy **215,** 271–280 (2004).
28. D. C. Ghiglia and M. D. Pritt. "Two Dimensional Phase Unwrapping. Theory, Algorithms and Software." Wiley, 1998.
29. M. Born and E. Wolf. "Principles of Optics". Pergamon Press, 6th edition, 1983.
30. R.J. Noll. "Zernike polynomials and atmospheric turbulence." J. Opt. Soc. Am. **66,** 207–277 (1976).
31. M. J. Booth and T. Wilson. "Refractive-index-mismatch induced aberrations in single-photon and two-photon microscopy and the use of aberration correction." J. Biomed. Opt. **6,** 266–272 (2001).
32. M.J. Booth. "Direct measurement of Zernike aberration modes with a modal wave front sensor." Proc. SPIE, Advanced Wavefront Control: Methods, Devices, and Applications **5162,** 79–90, 2003.
33. C. Paterson, I. Munro and J. C. Dainty "A low cost adaptive optics system using a membrane mirror" Opt. Express **6,** 175-185 (2000).
34. E.M.M. Manders, H. Kimura and P.R. Cook "Direct labelling of DNA in living cells reveals the dynamics of chromosome formation." J. Cell Biol. **144,** 813-823 (1999).

1. Introduction

Optical microscopes, including CFM and TPM, have become standard instruments in many life science laboratories. Modern microscopes are highly optimised and are designed to deliver a performance close to the physical diffraction limit. However, there is one element in the optical path that has a strong influence on the image quality but is hard to optimise: the specimen itself. A biological specimen may have, apart from absorption properties, a variation in refractive

#5762 - $15.00 US Received 17 November 2004; revised 13 December 2004; accepted 14 December 2004

index in the range from 1.30 to 1.50 [1, 2] and in some cases up to 1.70 [3]. If one intends to image details within a cell, the distribution of the refractive index in the obstructing layers above the focal region introduces aberrations. Aberrations have been subject to many investigations due to their detrimental effect on imaging quality [4-9]. In CFM [10, 11] and TPM [12] aberrations lead to reduced resolution and lower signal levels. It is clearly desirable to compensate for these effects in order to restore imaging quality and reduce phototoxicity arising from the use of unnecessarily high illumination power.

In this paper we describe the measurement and quantification of specimen induced aberrations from a number of biological specimens. Furthermore, using the examples of a CFM and TPM, we investigate the viability of low order aberration correction in high NA microscopy and the expected improvement in signal levels. In Table 1 the specimen types investigated, their approximate thickness, embedding medium and the corresponding scan ranges are listed.

Table 1. Specimen list (PBS : phosphate buffered saline, measurements approximate).

Specimen No.	Description	Embedding	Thickness [μm]	Lateral scan [μm]
1	brain tissue, rat	PBS	30	120×120
2	mouse oocyte	PBS	80	125×125
3	liver tissue, mouse	PBS	20	20×20
4	striated muscle, rat	PBS	40	50×50
5	C. elegans	Agar gel	40	50×50
6	vas deferens, rat	PBS	30	50×50

2. Adaptive optics for aberration correction

Aberrations can be removed by adaptive optics, a concept which is widely used in astronomy [13] where aberrations are introduced by refractive index variations in the atmosphere. In microscopy one attempts to image through an obstructing volume of inhomogeneous refractive index and possibly layers of mismatched refractive index. The idea of adaptive optics is to introduce conjugate aberrations that cancel out the aberrations arising within the system, thus recovering optimum, diffraction limited imaging. An adaptive optics system consists of a wavefront sensor (e.g. a Shack Hartmann sensor [14], an interferometer [13] or a modal wavefront sensor [15]) and a wavefront corrector (such as a deformable mirror [16-19] or a spatial light modulator (SLM)) that are combined in closed control loop. The principle of aberration correction has been demonstrated within a two photon microscope [19-22]. A more efficient implementation was incorporated into a CFM [23], where a single deformable mirror was used for both wavefront sensing and correction employing a modal wavefront sensing technique. Related systems have been implemented in ophthalmology using a deformable mirror in combination with a Shack-Hartmann sensor for imaging of the retina [18, 19]. Several theoretical investigations [5-9] were primarily concerned with spherical aberration arising from refractive index mismatch. However, biological specimens can have complicated variations in refractive index. The average refractive index of tissue or the refractive index of particular regions of biological specimens has been investigated [1-3] but relatively little information is available about the form and magnitude of aberrations introduced by complex biological specimens under high NA conditions. However, this information is essential for a systematic and directed approach to the design of an adaptive optical microscope.

#5762 - $15.00 US Received 17 November 2004; revised 13 December 2004; accepted 14 December 2004

3. Wavefront characterisation

Aberrations can be modelled by a complex pupil function

$$P(r,\theta) = A(r,\theta)\exp(j\psi(r,\theta)) \tag{1}$$

where $A(r,\theta)$ denotes the amplitude, $\psi(r,\theta)$ is the phase and $j = (-1)^{1/2}$. Using phase stepping interferometry [24-27]we can measure $A(r,\theta)$ and the wrapped phase function $\phi(r,\theta)$, where

$$\phi(r,\theta) = \psi(r,\theta) \bmod 2\pi. \tag{2}$$

The function $\psi(r,\theta)$ of the wavefront could then be recovered from $\phi(r,\theta)$, for example, using a phase unwrapping technique [28]. A convenient way to describe the aberrations is a series of Zernike polynomials, so that $\psi(r,\theta) = \sum_i M_i Z_i(r,\theta)$. The Zernike polynomials $Z_i(r,\theta)$ are a set of orthogonal functions defined over the unit circle and the lower orders correspond to the classical aberration terms such as spherical aberration, astigmatism and coma [29, 30]. The Zernike mode amplitudes, M_i, can be extracted from the unwrapped phase as

$$M_i = \frac{1}{\pi}\int_0^1 \int_0^{2\pi} \psi(r,\theta) Z_i(r,\theta)\, r\mathrm{d}\theta\mathrm{d}r. \tag{3}$$

Throughout this paper we use the indexing and normalization scheme of the Zernike polynomials as in [26] where all polynomials for $i > 1$ have a standard deviation of one radian over the unit circle. We can separate the Zernike modes into two classes: the first set consists of the Zernike modes tip ($i = 2$), tilt ($i = 3$) and defocus ($i = 4$). In a CFM they simply produce a displacement of the focal spot from its nominal position within the specimen. However, the image of the focal spot always falls on the pinhole detector since a conjugate displacement is introduced when the spot is re-imaged via the aberrating medium. In a sense, these modes are self correcting in a CFM but the displacement between the actual and nominal focal position in the specimen causes geometric distortion in the acquired three-dimensional image which can influence the accuracy of spatial measurements. This issue will be addressed in a future publication. The second class of modes ($i > 4$) changes the shape of the intensity distribution at the focal spot and influences signal level and resolution.

The quality of an optical system is often characterised by the Strehl ratio [29], which is defined as the ratio of the maxima of the focal intensity distributions for the aberrated and the unaberrated wavefront. We define the Strehl ratio as

$$S = \frac{|\int_0^1 \int_0^{2\pi} A(r,\theta)\exp(j\psi(r,\theta))rdrd\theta|^2}{(\int_0^1 \int_0^{2\pi} A(r,\theta)rdrd\theta)^2}. \tag{4}$$

This definition is slightly different from that in [29] and takes into account the amplitude variations. For moderate aberrations and especially if the wavefront contains only small amounts of the Zernike modes tip, tilt or defocus, equation (4) is equivalent to the ratio of the maximum focal intensity to the diffraction limited maximum intensity. Also, for small aberrations and no amplitude variations the Strehl ratio may be estimated from the variance of the wavefront [29] and finally the Zernike mode coefficients M_i as:

$$S \approx 1 - \mathrm{Var}(\psi(r,\theta)) = 1 - \sum_{i=5}^{\infty} M_i^2. \tag{5}$$

#5762 - $15.00 US Received 17 November 2004; revised 13 December 2004; accepted 14 December 2004

This is valid for $\mathrm{Var}(\psi(r,\theta)) \ll 1$.

The Strehl ratio can be related to the effective point spread function (PSF) in CFM and TPM. If we describe the focal distribution by the intensity PSF $h(x,y,z)$ then

$$S \equiv h(0,0,0)\ , \tag{6}$$

if $h(x,y,z)$ is normalized to the diffraction limited maximum intensity. In a CFM system with a vanishingly small pinhole, the effective PSF is the product of the illumination PSF, h_{il}, and emission PSF, h_{em} [31]. These would normally differ in scale because of the difference between the excitation and emission wavelengths. If we make the approximation that the fluorescence has the same wavelength as the illumination, then $h_{em} = h_{il}$ and the image of a point-like fluorescent object is given by

$$I_{CFM}(x,y,z) = h_{il}^2(x,y,z). \tag{7}$$

It is clear that the maximum signal is equivalent to S^2. In a TPM system that does not use a detection pinhole, the imaging depends only on the square of the illumination PSF [31] and the image of the fluorescent point object is described by

$$I_{TPM}(x,y,z) = h_{il}^2(x,y,z). \tag{8}$$

Again, the maximum signal is equivalent to S^2. Hence we can define the signal improvement factor, F_{sig}, for a CFM or TPM system to be:

$$F_{sig} = \left(\frac{S_{corr}}{S_{ini}}\right)^2. \tag{9}$$

Here S_{ini} denotes the initial Strehl ratio of the uncorrected wavefront and S_{corr} the Strehl ratio of the corrected wavefront. The value of F_{sig} represents the improvement in signal when aberration correction is applied to the excitation path of a TPM or the excitation and emission paths of a CFM using an infinitely small pinhole. This model of the imaging process allows us to estimate the potential benefit of adaptive optics in a straightforward manner. For small but finite sized pinholes in CFM, F_{sig} is expected to be similar. We note that the Zernike coefficients have units of phase and are therefore dependent upon wavelength. If no dispersion is present, the measured Zernike coefficients scale inversely with the wavelength. In this case it would be a simple matter to recalculate the factor of improvement for other wavelengths. The results shown assume an excitation wavelength of 633nm.

4. Experimental setup

We built a Mach-Zehnder phase stepping interferometer (Figure 1) to measure the aberrations induced by various specimens. The expanded He-Ne (633 nm) laser beam was split into reference and object paths. The specimen was placed in the object path between two opposing water immersion lenses (Carl Zeiss C-Apochromat, 63x Korr, NA=1.2) that were equipped with cover glass correction collars. A rotation of the $\lambda/2$-plate in front of the polarising beamsplitter permitted the adjustment of the relative intensities of the two paths. When the object beam traversed the specimen it was made to interfere with the reference beam and the resulting interference pattern was recorded on a CCD camera. The image plane of the CCD was conjugate to the pupil plane of the second objective lens. The phase stepping unit placed in the

#5762 - $15.00 US Received 17 November 2004; revised 13 December 2004; accepted 14 December 2004

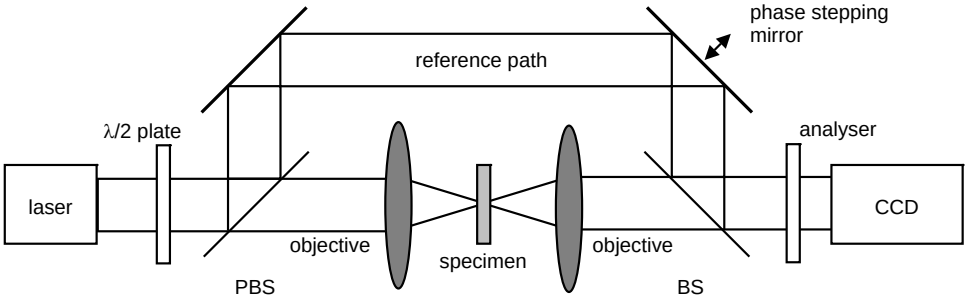

Fig. 1. Phase stepping interferometer for aberration measurement (see text). (PBS - polarising beam splitter, BS - beam splitter.) The specimen is mounted between two opposing high NA lenses and scanned laterally by means of a computer controlled stage. Some intermediate lenses have been omitted for clarity.

reference beam path took the form of a flat mirror mounted on a calibrated piezo drive. This allowed us to change the relative phase between reference and object beams in well defined steps. The phase stepping was synchronised with the CCD-camera and digital interferogram images were recorded using a framegrabber. The specimen was attached to a piezo driven stage that could be positioned in three dimensions. Furthermore, for specimen navigation, the object path could be switched to operate as a conventional transmission microscope using an additional CCD camera and illumination elements (not shown in the Figure).

Because of the short working distance of the high NA lenses the specimen had to be mounted between two coverslips. The coverslip correction collars of the lenses were set to minimize the first order spherical aberration coefficient M_{11} when focussing through the coverslip and mounting medium adjacent to the specimen. Ideally, one should measure the absolute change in phase introduced by the specimen. In practice, small residual aberrations might be introduced by the optical system and were removed by the following calibration step. For each specimen, calibration measurements were taken by focussing adjacent to the specimen. All subsequent wavefronts were measured relative to this calibration reference. It is possible that some specimen induced spherical aberration was removed by this step (or introduced by the correction ring collars). However, this still permitted the measurement of the variation of the spherical aberration across the specimen and the introduction of spherical aberration by a refractive index mismatch is well known [4, 7, 9]. Since some static, uncompensated spherical aberration may be present the real aberrations might in fact be worse than that measured here.

The CFM is usually implemented in an epi configuration, where aberrations are introduced in the excitation and emission optical paths between the lens and the focal spot, whereas our interferometer measured aberrations in transmission for a single pass through the specimen. Therefore, one has to be aware that the aberrations measured are strictly equivalent to the epi case only when the focus is set to the bottom of the specimen. Then no further aberrations are introduced beyond the focal spot. This limitation is not severe since the strongest aberrations may occur when the whole specimen is traversed and we are interested in this situation to estimate the maximum correction range an adaptive optics system needs to provide. For all of our measurements the focus was set to the bottom of the specimen.

#5762 - $15.00 US Received 17 November 2004; revised 13 December 2004; accepted 14 December 2004

5. Data acquisition

One data set consists of 256 wavefront recordings corresponding to focal positions arranged on a 16×16 square grid across the specimen. For each wavefront a set of three interferograms at different relative phase steps were recorded and the amplitude $A(r,\theta)$ and the wrapped phase $\phi(r,\theta)$ of the wavefront were calculated [26]. In Figure 2 the transmitted light image and the wavefront disturbance (video) are shown as the focal spot was scanned across specimen number 5 (C. elegans). In the next step, the Zernike mode components were extracted from each of the

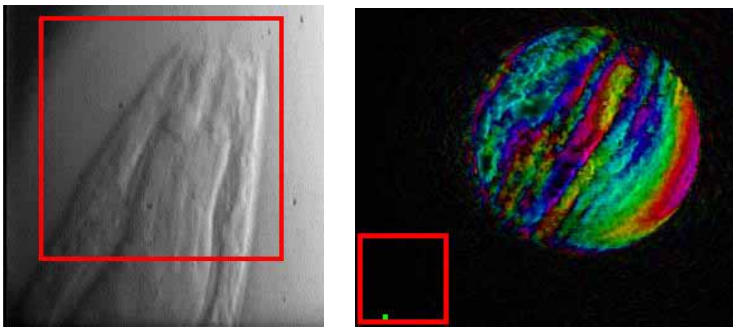

Fig. 2. Left: transmitted light image of the specimen number 5 (C. elegans). The red box indicates the scanned region of 50×50 μm. Right: video of the disturbance of the wavefront in the pupil plane of the lens as the focal spot scans across the specimen. Here the complex wavefront consisting of the amplitude $A(r,\theta)$ and the wrapped phase function $\phi(r,\theta)$ is displayed. The color encodes the phase whereas the brightness corresponds to the amplitude of the wavefront. The green dot within the red frame in the lower left corner of the video indicates the relative position within the scanned area. (AVI-video file, size 2.4 MB.)

wavefronts using a procedure of phase unwrapping that gives the Zernike coefficients directly. It is based on modal wavefront sensing described in [15, 23, 32]. First a positive bias of $+b_iZ_i$ of the particular Zernike mode Z_i one intends to measure is added to the original wavefront ϕ. Then the Strehl ratio $S(\phi + b_iZ_i)$ is calculated. Now a negative bias of the same magnitude $-b_iZ_i$ is added to the original wavefront and $S(\phi - b_iZ_i)$ is computed. One can show [32] that the amplitude of the Zernike mode Z_i contained in the original wavefront is proportional to the quantity $S(\phi + b_iZ_i) - S(\phi - b_iZ_i)$. This procedure is repeated until the modal amplitude of all Zernike modes up to $i = 22$ are measured. It is a simple matter now to remove an amount of Zernike mode Z_i from the original wavefront. The procedure is iterated until no further improvement in Strehl ratio is detected. This simulates the operation of modal wavefront sensing and correction. An advantage of this method is that the Zernike data is extracted directly from the wrapped phase data $\phi(r,\theta)$ that was measured and so we do not require an intermediate phase unwrapping process. Furthermore we found that this method performed better than other phase unwrapping methods for the analysis of this data.

6. Results

Figure 3 displays examples of measured wavefronts (top) and their simulated correction (bottom) up to Zernike mode 22. Inset (1) shows an interferogram from rat brain tissue, 30 μm thick, covering half of the pupil. Two effects are visible: a rather strong spherical aberration component (note the coloured rings at the edge of the top half of the pupil) is introduced and

#5762 - $15.00 US Received 17 November 2004; revised 13 December 2004; accepted 14 December 2004

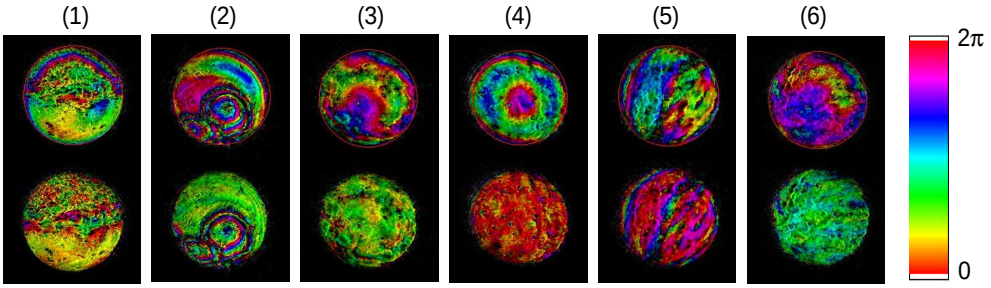

Fig. 3. Specific interferogram examples from a particular position within the 16×16 grid that was recorded for each specimen. The color encodes the phase, the brightness corresponds to the amplitude. The numbers (1) to (6) are the specimen numbers listed in Table 1; The upper part shows the measured initial wavefront, the lower part a simulated correction of the Zernike modes up to $i = 22$.

a modulation of the phase function with high spatial frequencies is visible. The Zernike based approach can correct for the lower order terms but cannot correct the high spatial frequency components; a partial correction is achieved and can be considered optimal for the modes included in the correction. This method worked well for 30μm thick brain slices. However, for thicker brain specimens of about 90 μm (data not shown) the aberration appeared to be dominated by high spatial frequency variations that could not be removed by a small number of modes. In (2) some of the structure of the mouse oocyte is visible in the pupil. There is sudden change of phase accompanied by amplitude effects at the cell boundaries. Again partial correction was achieved which can be considered optimal within the modes included. The mouse liver wavefront shown in (3) exhibits strong but rather smooth disturbance and good correction was achieved. In (4) the sample of striated muscle is shown. A rather smooth disturbance is present that can be well corrected with a low order Zernike modal approach. In this case a large amount of spherical aberration, probably arising from the refractive index mismatch, was removed in the calibration step. Image (5) shows a heavily aberrated wavefront from the C. elegans specimen. The smooth muscle tissue wavefronts are depicted in (6); the phase disturbance contained mainly low order Zernike terms and the almost uniform color (lower part) indicates very good phase correction.

After the Zernike mode extraction, each coefficient M_i may be represented as Zernike mode pseudo image that shows the variation of M_i as one scans across the specimen. Figure 4 displays an example for the C. elegans specimen. Here modes 5 to 12 are depicted. The total Zernike figure is calculated using $(\sum_{i=5}^{22} M_i^2)^{1/2}$.

For the purpose of designing and implementing adaptive optics it is important to consider the variations of the aberrations across the field of view. The mean and standard deviation for each mode was calculated from maps such as shown in Figure 4; a result for the C. elegans is displayed in Figure 5. The Zernike mode standard deviation declines with rising order. This general behavior was found for all the specimens. The aberration effect that is contributed from the individual coefficients is proportional to the square of the Zernike mode amplitude, as can be inferred from equation (5). Thus the influence of the higher order modes could be considered to decline even faster than the amplitudes shown in Figure 5. The magnitude of the Zernike mode amplitudes of all specimens were within the range of up to 1.5 for the modes 5 to 11. Maximum magnitudes smaller than 1 Zernike unit were observed for modes from 12 to 22, and for modes above 22 all magnitudes were smaller than 0.5.

#5762 - $15.00 US Received 17 November 2004; revised 13 December 2004; accepted 14 December 2004

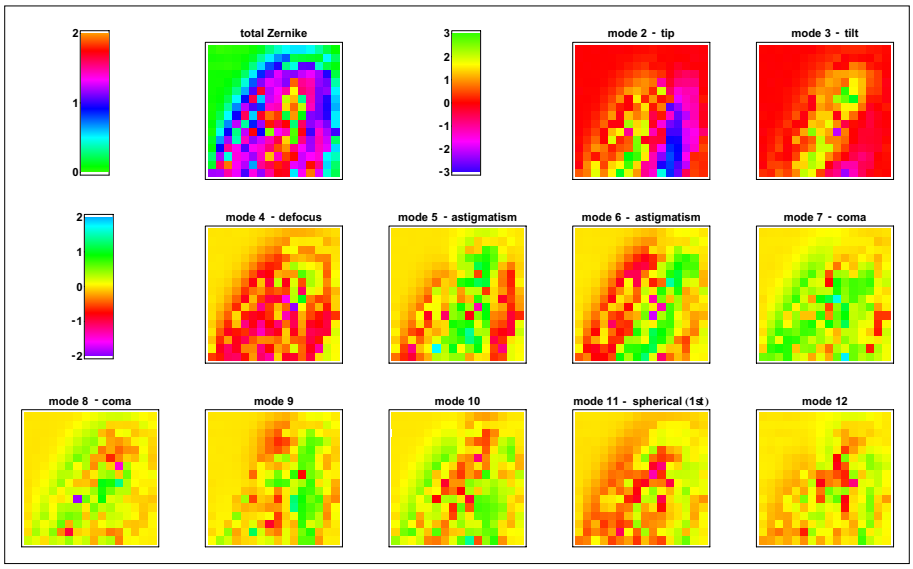

Fig. 4. Zernike mode pseudo images of the specimen specimen number 5, C. elegans. The Zernike mode amplitudes M_i of the modes 2 to 12 (in Zernike mode units, see definition in equation 3) are depicted.

In addition we are also interested to assess the potential benefit of aberration correction. We simulated Zernike mode based correction and calculated the Strehl ratios of the wavefronts before (S_{ini}) and after the correction (S_{corr}). Modes 2 to 4 do not affect the signal in an epi-CFM system. Therefore these modes were subtracted from the raw wavefront prior to the Strehl ratio

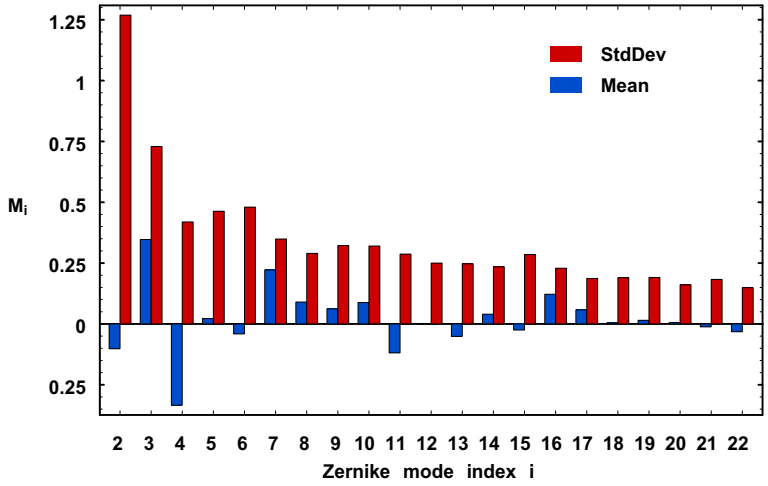

Fig. 5. Mean and standard deviation of the Zernike mode amplitudes, in Zernike mode units, for the C. elegans - specimen 5. The modes 2 to 22 are shown.

#5762 - $15.00 US Received 17 November 2004; revised 13 December 2004; accepted 14 December 2004

calculations. In order to exclude the effect of static aberration that may be caused by imperfections of the optical system itself, the Zernike mode components for modes $i \geq 5$ obtained from the calibration wavefront recorded next to the sample were also subtracted. The Strehl ratio S_{ini} was calculated for the resulting wavefront from equation (4). A second Strehl ratio S_{corr} was calculated for a wavefront where the Zernike modes obtained in the analysis were subtracted from the measured raw wavefront. This simulated the correction of the wavefront for a certain number of modes.

Table 2. Correction benefit for different degrees of correction.

Specimen Number	Correction up to mode	Mean S_{ini}	Mean S_{corr}	Mean F_{sig}	Median F_{sig}
1	12	0.40	0.49	4.47	1.80
	18	0.40	0.54	5.50	2.24
	22	0.40	0.65	7.57	3.48
	37	0.40	0.66	7.88	3.81
2	12	0.47	0.51	4.00	1.10
	18	0.47	0.58	6.13	1.38
	22	0.47	0.62	6.27	1.63
	37	0.47	0.65	7.02	1.78
3	12	0.32	0.52	5.30	2.90
	18	0.32	0.57	6.35	3.36
	22	0.32	0.65	7.84	4.39
	37	0.32	0.72	8.98	5.79
4	12	0.48	0.63	2.15	1.86
	18	0.48	0.78	3.13	2.58
	22	0.48	0.81	3.35	2.76
	37	0.48	0.84	3.66	2.97
5	12	0.46	0.59	7.31	1.29
	18	0.46	0.60	7.13	1.39
	22	0.46	0.71	9.65	1.98
	37	0.46	0.78	12.66	2.28
6	12	0.47	0.58	1.83	1.47
	18	0.47	0.62	2.11	1.69
	22	0.47	0.72	2.80	2.27
	37	0.47	0.77	3.21	2.64

The results for the mean initial Strehl ratio, the mean corrected Strehl ratio, and the mean and median of the confocal F_{sig} are summarised in Table 2 where the specimen numbers used are defined in Table 1. In order to investigate the interplay between the correction quality and the number of corrected Zernike modes we calculated simulations up to modes 12, 18, 22 and 37 for all the specimens. In general, the correction of up to 37 modes was found to give only moderate improvement in the Strehl ratio compared to the correction of 22 modes. It appears that for these specimens the correction of 22 or even 18 Zernike modes is a good compromise between the effort required for the correction and the improvement in Strehl ratio. Maps of the Strehl parameters are shown Figure 6, the specimens are again denoted by the numbers listed in Table 1. Significant spatial variations of the initial Strehl ratio are evident in all specimens. It is

#5762 - $15.00 US Received 17 November 2004; revised 13 December 2004; accepted 14 December 2004

important to note this phenomenon. The measured intensity displayed in a standard CFM image is normally regarded as a quantity that represents fluorophore concentration. Our results indicates that aberrations and not just the fluorophore concentration affect the measured intensity. This has important implications for quantitative fluorescence microscopy.

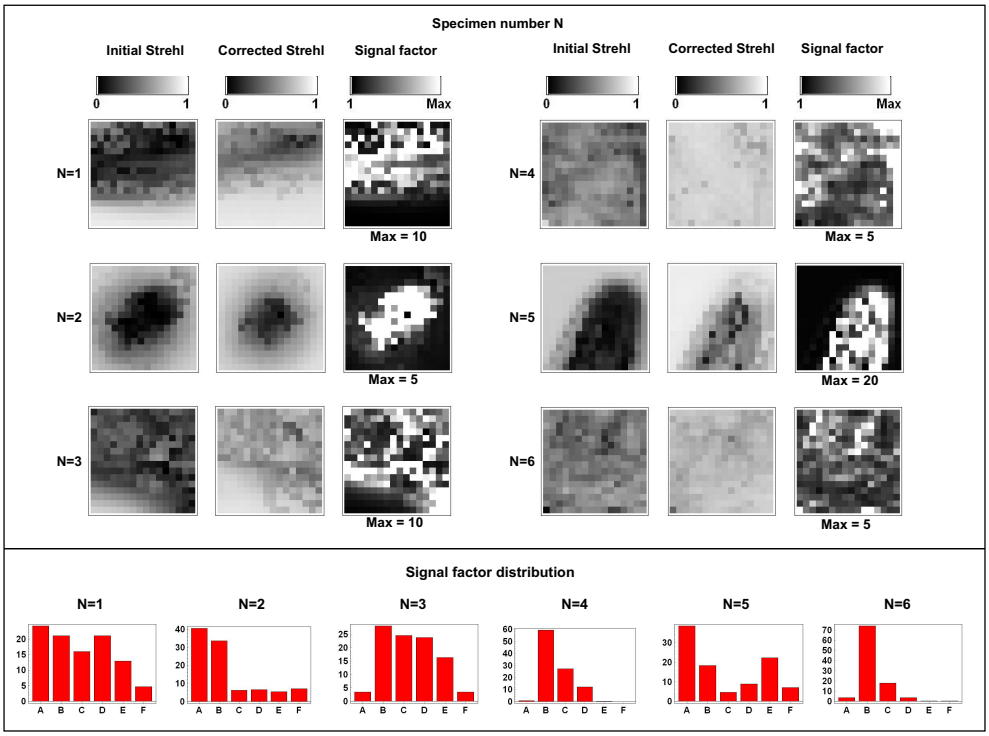

Fig. 6. Maps of the initial Strehl ratio S_{ini}, the Strehl ratio S_{corr} after correction up to Zernike mode 22, and the derived signal correction factor F_{sig}. The distribution of F_{sig} is shown in a histogram for each of the specimens. The non-uniform histogram intervals are: A:[0, 1.5); B:[1.5, 3); C:[3, 5); D:[5, 10); E:[10, 40); F: [40,∞]. The vertical axis shows percentage of pixels within the range. The maximum of the range for each F_{sig} plot is shown below the plot and values larger than this maximum are shown in white.

We note that in some cases the specimen does not fill the whole field of view and F_{sig} is smaller in the areas adjacent to the specimen. The calculated mean F_{sig} was typically in the range between 2 and 10 for a correction of the Zernike modes 5 to 22. The median value is listed as this tends to be less sensitive to extreme values.

Another aspect investigated was the influence of the NA on the size of the aberrations and the benefit of modal adaptive correction. Wavefront data for different numerical apertures can be extracted from the interferograms by analysing an aperture subregion of smaller radius. Our data sets were recorded with a physical NA of 1.2 and data analysis was performed for the numerical apertures 1.2, 0.9 and 0.6 for a correction up to Zernike mode 37; the results are listed in Table 3 (see Table 1 for specimen numbers). The magnitude of aberrations, especially higher orders, increases with NA. As an example the phase function corresponding to spherical aberration [7-9] rises sharply towards the edge of a high NA pupil. Since a lower NA objective accepts only the central portion, the effects of spherical aberration are correspondingly reduced.

#5762 - $15.00 US Received 17 November 2004; revised 13 December 2004; accepted 14 December 2004

The dependence of other, higher order aberration modes is conceptually similar. Therefore, in a low NA system, the aberrations tend to be smaller in amplitude and the initial Strehl ratio is correspondingly higher. This is supported by the experimental results. As a consequence the benefit of correction for lower NA was found to be smaller. For the particular case of the mouse oocyte (specimen 2), the mean of F_{sig} for NA=0.6 is largest but this is because of a few locations with very large values of F_{sig}. However, the median value of the distribution for NA=0.6 is lower than that for the higher numerical apertures.

Table 3. Correction benefit at different numerical apertures.

Specimen Number	NA	Mean S_{ini}	Mean S_{corr}	Mean F_{sig}	Median F_{sig}
1	1.2	0.40	0.66	7.88	3.81
	0.9	0.62	0.76	2.24	1.37
	0.6	0.70	0.82	1.81	1.18
2	1.2	0.47	0.65	7.02	1.78
	0.9	0.55	0.73	6.18	1.58
	0.6	0.60	0.79	9.02	1.49
3	1.2	0.32	0.72	8.98	5.79
	0.9	0.63	0.85	2.16	1.59
	0.6	0.78	0.90	1.42	1.33
4	1.2	0.48	0.84	3.66	2.97
	0.9	0.60	0.85	2.19	1.98
	0.6	0.75	0.92	1.57	1.49
5	1.2	0.46	0.78	12.66	2.28
	0.9	0.64	0.87	4.15	1.68
	0.6	0.75	0.90	2.32	1.07
6	1.2	0.47	0.77	3.21	2.64
	0.9	0.66	0.84	1.71	1.58
	0.6	0.76	0.89	1.40	1.29

7. Discussion

We can conclude: specimen induced aberrations lead to reduced signal levels and a deterioration in image quality in optical microscopy, especially in CFM and TPM. For the first time, specimen induced aberrations that occur with various biological specimens have been classified and quantified for the most relevant condition of high NA. The above approach can provide detailed information about the variation of each Zernike coefficient across the scan. This could also deliver information about the temporal dynamics of the aberrations due to the scanning of the focal spot through the specimen. Our calculation of the correction benefit is based on the assumption that a correction would be applied at every position within the scanned area. The feasibility of this assumption depends on the bandwidth of the wavefront sensing and correction devices and the scan speed. In some cases it may be required to either reduce the scan speed or update the aberration correction every few pixels only.

In a practical AO system that employs a deformable mirror other sets of orthogonal modes, for example the mirror deformation eigenmodes [33], may be more appropriate as a basis for

#5762 - $15.00 US Received 17 November 2004; revised 13 December 2004; accepted 14 December 2004

correction. It is generally straightforward to convert from one representation to another.

The measurements indicate significant variations of the uncorrected Strehl ratio throughout the specimen, which could influence quantitative fluorescence measurements in an uncorrected system. We showed that low order aberration correction based on Zernike modes will provide significant recovery of signal levels in CFM and TPM, even if the diffraction limit is not restored. For the six specimens examined, the mean F_{sig} was in the range between 2 and 10 for a correction of the Zernike modes 5 to 22 at an NA of 1.2. Note that the quoted values refer to frame averages and the factors in specific areas might be even higher. It should be pointed out that the set of biological specimens investigated is necessarily incomplete and differences between biological specimens can be large. However, the benefit found for these specimen would be highly significant in CFM and TPM since light budgets are typically tight and efficient use of available photons is crucial to minimise photobleaching and phototoxic effects [34].

As expected from theory, lower NA systems are less susceptible to aberrations than high NA system under otherwise similar conditions. Low order correction would still provide benefits, even though the initial aberrations are smaller. The results presented here quantify the benefit of adaptive optics for biological microscopy and provide the bounds within which these systems must operate.

Acknowledgments

We would like to thank the following for providing specimens: Richard Gardner and Tim Davis, Dept. of Zoology, Oxford; Allison Woollard, Dept. of Biochemistry, Oxford; Tom Cunnane, Keith Brain and Patricia Tynan, Dept. of Pharmacology, Oxford. This work was supported by Carl Zeiss Jena GmbH and Research Councils UK under the Basic Technology scheme. M.S. is supported by the DAAD Germany (German Academic Exchange Service). M.J.B. is a Royal Academy of Engineering / EPSRC Research Fellow.

#5762 - $15.00 US Received 17 November 2004; revised 13 December 2004; accepted 14 December 2004